

Cross-Modal Consistency Learning for Sign Language Recognition

Kepeng Wu¹, Zecheng Li¹, Weichao Zhao¹, Hezhen Hu³, Wengang Zhou^{1,2,*}, Houqiang Li^{1,2}

¹MoE Key Laboratory of Brain-inspired Intelligent Perception and Cognition,
University of Science and Technology of China

²Institute of Artificial Intelligence, Hefei Comprehensive National Science Center

³University of Texas at Austin

{wukp, lizecheng23, saruka}@mail.ustc.edu.cn

{zhwg, lihq}@ustc.edu.cn, alexhu@utexas.edu

Abstract

Pre-training has been proven to be effective in boosting the performance of Isolated Sign Language Recognition (ISLR). Existing pre-training methods solely focus on the compact pose data, which eliminate background perturbation but inevitably suffer from insufficient semantic cues compared to raw RGB videos. Nevertheless, direct representation learning only from RGB videos remains challenging due to the presence of sign-independent visual features. To address this dilemma, we propose a Cross-modal Consistency Learning framework (CCL-SLR), which leverages the cross-modal consistency from both RGB and pose modalities based on self-supervised pre-training. First, CCL-SLR employs contrastive learning for instance discrimination within and across modalities. Through the single-modal and cross-modal contrastive learning, CCL-SLR gradually aligns the feature spaces of RGB and pose modalities, thereby extracting consistent sign representations. Second, we further introduce Motion-Preserving Masking (MPM) and Semantic Positive Mining (SPM) techniques to improve cross-modal consistency from the perspective of data augmentation and sample similarity, respectively. Extensive experiments on four ISLR benchmarks show that CCL-SLR achieves impressive performance, demonstrating its effectiveness. The code will be released to the public.

1. Introduction

Sign language, which combines body gestures and facial expressions to convey semantic meaning, serves as the primary communication tool within the Deaf community. To facilitate a barrier-free understanding between sign language and spoken language, extensive research [13, 16, 17,

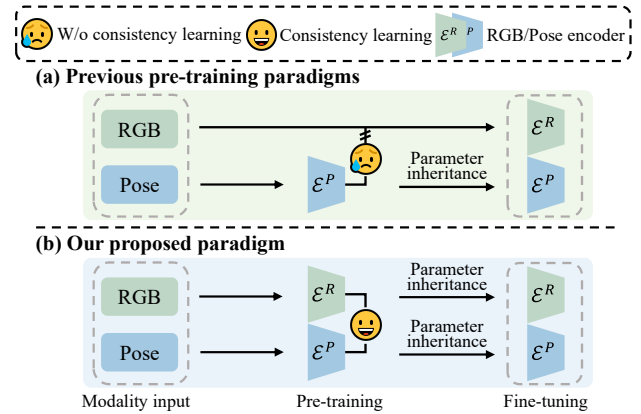


Figure 1. Comparison between previous pre-training paradigms and ours. (a) Previous paradigms [13, 16, 46, 48] ignore modeling the interaction between RGB and pose modalities during pre-training. (b) Our proposed method effectively aligns embedding spaces of two modalities via cross-modal consistency learning.

21, 28, 44, 46, 48, 55] has explored sign language understanding from various perspectives. Isolated Sign Language Recognition (ISLR) is a fundamental task in sign language understanding, which focuses on recognizing the meaning of sign language videos at the word level to achieve fine-grained understanding. For the deployment of ISLR models in real-world applications, developing robust visual encoders with enhanced representation capabilities has increasingly been recognized as a crucial research direction.

Current ISLR methods mainly employ supervised paradigms on small-scale dataset [15, 18, 24, 26], which can be categorized into two paradigms based on the input modalities. (1) RGB-based methods [14, 15, 17, 24–29, 44] explore various strategies to extract discriminative visual features from RGB videos. Although these methods are intuitive and straightforward, they fail to explicitly cap-

*Corresponding author

ture key gesture-related information. Furthermore, signer-dependent variations hinders effective feature extraction, ultimately compromising the robustness of the sign representations. (2) Pose-assisted methods [20, 21, 55] integrate the pose modality and employ multi-stream fusion frameworks to leverage cross-modal complementary information. By utilizing the compact pose modality, these methods efficiently eliminate non-skeletal noise. However, current pose data is directly derived from pose extractors trained on general domain data distributions. Due to motion blur and hand occlusion in sign language videos, these general extractors inevitably produce errors and missing detection, limiting the performance ceiling of these pose-assisted methods.

Although these supervised methods have achieved promising results, the scarcity of labeled training data inherently constrains their representation and generalization capabilities. To tackle this problem, recent works [13, 16, 46–48] attempt to explore self-supervised pre-training strategies in the pose modality to enhance visual modeling capabilities. For instance, MASA [47] propose a motion-aware masked auto encoder to utilizes the pose modality by introducing a motion prior and global semantic cues into pre-training. However, it only incorporate RGB information by late fusion in fine-tuning, failing to leverage original RGB features during pre-training. As shown in Fig. 1(a), these self-supervised methods focus solely on extracting visual information from pose modality. This paradigm fails to consider cross-modal feature interactions and overlooks the potential benefits of original RGB visual information.

In this paper, we aim to introduce cross-modal consistency learning into the pre-training paradigm to fully enhance feature extraction in subsequent stages. Notably, effectively applying self-supervised paradigms such as contrastive learning to cross-modal interaction is non-trivial due to two key challenges: (1) **Redundant information in the RGB modality.** RGB images contain redundant non-semantic information in background regions, such as signer-dependent variations such as body type and skin color, which are often irrelevant to pose information. These redundant cues interfere with the feature extraction of sign language-related cues, further impacting the ISLR performance. (2) **Inconsistency between modalities.** Although the RGB and pose data of the same instance correspond to each other, the similarity structural relationships between instances across the two modalities are inconsistent, which leads to the inherent misalignment in feature distributions across RGB and pose modalities.

To this end, we propose a novel Cross-modal Consistency Learning framework (CCL-SLR), which aims to model consistency constraints during pre-training, as shown in Fig. 1 (b). We employ single-modal contrastive learning and cross-modal contrastive learning to facilitate instance discrimination within individual modalities and across dif-

ferent modalities, respectively. To more effectively extract consistent sign language representations from both RGB and pose modalities in the contrastive learning paradigm, our approach incorporates two key modules: Motion-Preserving Masking (MPM) and Semantic Positive Mining (SPM). (1) **To eliminate impact from redundant features,** MPM introduces an off-the-shelf flow-based model to extract latent representations, leveraging this information to capture motion dynamics. By preserving motion-related information, MPM suppresses non-semantic regions in RGB videos, thereby enhancing the relevance of learned features. (2) **To capture cross-modal structural consistency,** SPM identifies semantically similar samples within each modality to provide pseudo-supervision for both modalities. Through a multi-label classification approach, this pseudo-supervision introduces shared positive constraints across different modalities, effectively bridging the distribution gap between them. To validate the effectiveness of our method, we conduct extensive experiments on four widely adopted ISLR benchmarks. In summary, our contributions are as follows:

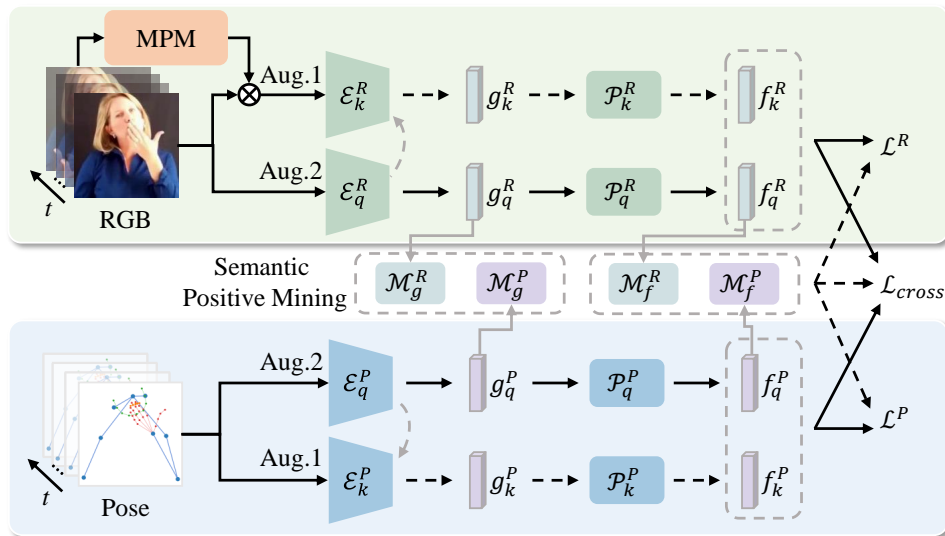
- We propose a novel pre-training framework named CCL-SLR, which effectively leverages the single-modal and cross-modal contrastive learning on both RGB and pose modality for enhancing ISLR.
- We introduce MPM and SPM, two innovative techniques designed to mitigate the distribution gap between modalities and further strengthen the consistency constraints during cross-modal pre-training.
- We conduct extensive experiments on four widely-adopted benchmarks and achieve impressive performance, which demonstrates effectiveness and representation capability of CCL-SLR.

2. Related Work

Sign Language Recognition. Sign language recognition is a subtask in field of sign language understanding, which aims to recognize single sign word within a given video. Early works [6, 7, 32, 34, 37] utilize hand-craft feature to model spatio-temporal representation. With development of deep convolution neural networks (CNNs), numerous recent works [14, 15, 24–27, 29] leverage CNN-based architectures such as TSM [30], R3D [10] and I3D [1] to extract visual representation from RGB videos. For example, StepNet [36] use TSM to model part-level spatial and temporal relationship, achieving impressive performance on ISLR.

However, these RGB-based methods may suffer from static irrelevant cues in sign language videos [55], such as background and clothing. Consequently, several works begin to explore pose-assisted method, trying to utilize the effectiveness of compact sign pose data. For instance, NLA-SLR [55] present a video-keypoint multi-stream backbone and utilize semantic information within sign glosses to pro-

(a) Overview of pre-training framework



(b) Semantic Positive Mining

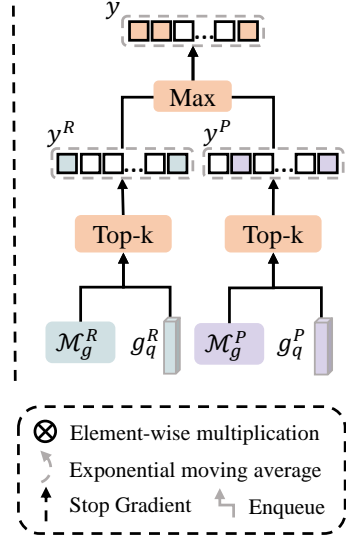


Figure 2. (a) The CCL-SLR pre-training framework. RGB and pose sequences are processed through two single-modal branches to learn modality-specific representation. During this process, MPM is applied to mask motion-irrelevant regions in RGB videos. Additionally, cross-modal positive samples are identified through SPM, which are utilized for \mathcal{L}^R and \mathcal{L}^L . Finally, the consistency of RGB and pose embedding spaces is constrained through \mathcal{L}_{cross} . (b) An overview of SPM. SPM selects the top-k most similar samples from each modality-specific memory bank and merges them to form pseudo-labels.

mote ISLR. SAM-v2 [21] jointly leverage pre-extracted multi-modal data with a branching ensemble model to achieve higher recognition rate. Although these works effectively fuse RGB and pose modality features, they rely on complex model designs and feature fusion strategies, which affect their scalability. Meanwhile, some studies [13, 16, 46–48] incorporate self-supervised pre-training paradigms into ISLR to address the challenge of data scarcity. SignBERT [13] enhance model representation capacity through generative pretext task specifically designed for pose data during self-supervised pre-training. BEST [46] leverage discrete variational autoencoder to compress hand shapes into a codebook for implicit clustering, serving as pseudo-labels to better learn skeletal priors. Nevertheless, these approaches overlook the benefits of aligning consistency visual representations of RGB and pose data during the pre-training for downstream ISLR tasks.

In this work, we focus on ISLR pre-training paradigm, learning instance discriminative representations through contrastive learning within and across modalities.

Contrastive Representation Learning. Contrastive learning has significantly advanced self-supervised visual representation learning by performing instance discrimination in a fully self-supervised manner [2, 3, 8, 11, 33, 43]. It pulls positive samples closer and pushes negative samples away. Since there are no supervised labels, different data augmentations of the same instance are treated as a positive pair, while samples from other instances are used as

negative pairs. Recently, MoCo [11] and MoCo v2 [3] strengthens contrastive learning by maintaining a dynamic memory bank of negative sample embeddings from previous iterations. Based on them, current advances have demonstrated substantial improvements in representation capability through various technical innovations, including positive mining [19, 42, 52, 54] and data augmentation [5, 38, 45, 53].

Although these methods have achieved success in various downstream tasks, incorporating the contrastive learning paradigm into multi-modal ISLR pre-training remains a challenge. To this end, we propose CCL-SLR, which attempts to extend the MoCo v2 framework to the challenging task of cross-modal sign language representation learning.

3. Method

As illustrated in Fig. 2, our framework first applies the modality-specific data augmentation to generate augmented samples. Subsequently, these augmented samples are processed through their respective encoders for feature extraction. The encoder outputs are then utilized to compute the contrastive loss, facilitating the learning of instance discriminative representations within and across modalities. For the RGB modality, we introduce a novel Motion-Preserving Masking mechanism to mitigate redundant non-semantic visual cues in the RGB video. Furthermore, to enhance the single-modal discriminative representation learn-

ing while leveraging the cross-modal consistency, we propose a Semantic Positive Mining mechanism that identifies semantically similar positive sample pairs.

3.1. Preliminaries

Single-modal contrastive learning has emerged as a powerful paradigm in diverse tasks, with notable success demonstrated by MoCo v2 [3]. For a given single-modal input x in a mini-batch, the learning process begins with data augmentation to generate two distinct samples x_q and x_k (query and key). Then, two encoders, \mathcal{E}_q and \mathcal{E}_k , are applied to embed x_q and x_k into a hidden space:

$$z_q = \mathcal{E}_q(x_q; \theta_q), \quad z_k = \mathcal{E}_k(x_k; \theta_k), \quad (1)$$

where \mathcal{E}_q and \mathcal{E}_k denote the query and key encoders, θ_q and θ_k denote the learnable parameters of the encoders. Notably, the key encoder \mathcal{E}_k is maintained as an exponential moving average (EMA) of the query encoder \mathcal{E}_q , updated as: $\theta_k \leftarrow \gamma \theta_k + (1 - \gamma) \theta_q$, where γ denotes the momentum coefficient. During the pre-training phase, instance discrimination is achieved through the InfoNCE [39] loss:

$$\mathcal{L}_{cl}(z_q, z_k, \mathcal{S}) = -\log \frac{\exp(z_q \cdot z_k / \tau)}{\exp(z_q \cdot z_k / \tau) + \sum_{s_i \in \mathcal{S}} \exp(z_q \cdot s_i / \tau)}, \quad (2)$$

where τ represents the temperature coefficient [12], and \mathcal{S} denotes the negative sample embedding set maintained in a memory bank of size N . The similarity between samples is computed using the dot product operation.

3.2. Single-Modal Contrastive Learning

Framework Architecture. As illustrated in Fig. 2, CCL-SLR consists of two parallel single-modal branches: an RGB branch and a pose branch. Each branch encompasses two pathways for key and query sample, along with two queue-based memory banks. Each pathway consists of an encoder and a projection head. Since recent ISLR datasets do not provide pose annotation, we first extract the corresponding pose sequence $X^P \in \mathbb{R}^{T \times J \times C_p}$ using an off-the-shelf estimator [4] from RGB frame sequence $X^R \in \mathbb{R}^{T \times H \times W \times 3}$. Here, T denotes the frame length, J denotes the number of joints, while H and W correspond to the spatial dimensions. C_p represents XY coordinates with confidence of pose data.

First, we use spatial-temporal augmentation to generate different query and key sample for single-modal branches, denoted as X_s^m , where $m \in \{R, P\}$ represents RGB and pose modality and $s \in \{q, k\}$ represents query and key samples. Second, each sample X_s^m is processed by its corresponding encoder \mathcal{E}_s^m to obtain embedding $g_s^m \in \mathbb{R}^d$. The RGB encoder employs R3D-50 [10] backbone, while the pose encoder utilizes a GCN+Transformer architec-

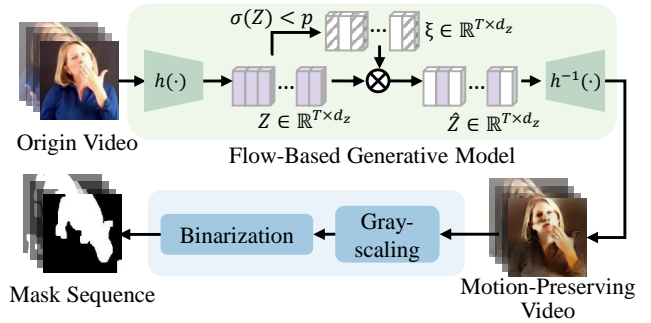


Figure 3. An overview of MPM. Here $h(\cdot)$ and $h^{-1}(\cdot)$ denotes the transformation from pixel/latent space to latent/pixel space, respectively. The original video is encoded into latent space using a flow-based generative model. Channels in the latent representation with low standard deviation along temporal dimension are then masked out. The masked latent representation is decoded back into pixel space. The reconstructed frames are then processed through gray-scaling and binarization to produce motion-aware mask sequence.

ture [50]. Then, g_s^m is projected using multi-layer perceptron (MLP) projection head \mathcal{P}_s^m to obtain the final embedding $f_s^m \in \mathbb{R}^d$. Two queue-based memory banks $\mathcal{M}_g^m \in \mathbb{R}^{N \times d}$ and $\mathcal{M}_f^m \in \mathbb{R}^{N \times d}$ are utilized for storing L2 normalized embeddings of g_s^m and f_s^m , respectively:

$$\|g_k^m\|_2 \xrightarrow{\text{Enqueue}} \mathcal{M}_g^m, \quad \|f_k^m\|_2 \xrightarrow{\text{Enqueue}} \mathcal{M}_f^m, \quad (3)$$

where $\|\cdot\|_2$ denotes the L2 normalization operation. Here, \mathcal{M}_g^m is utilized to mine semantic positive samples, and \mathcal{M}_f^m is applied for contrastive learning.

Motion-Preserving Masking (MPM). Unlike pose sequence that focuses on keypoint coordinates, RGB video contains substantial non-gestural information such as background and clothing. To preserve essential motion components while suppressing irrelevant regions, we propose MPM, an augmentation that enhances motion capture capabilities and mitigates bias from non-skeleton elements. For mapping RGB videos from pixel space to a compact feature space, MPM employs a pre-trained flow-based generative model, AdvFlow [31] for motion-preserving latent representation extraction.

Given an RGB video X^R , we encode it into latent representation $Z \in \mathbb{R}^{T \times d_z}$. Empirically, the temporal standard deviation of each channel serves as an indicator of its motion information content. We apply this measure to Z to preserve dynamic features while suppressing static ones:

$$\hat{Z} = Z \otimes \mathbb{1}(\sigma(Z) < p), \quad (4)$$

where $\mathbb{1}(\cdot)$ denotes the indicator function, $\sigma(\cdot)$ computes the standard deviation along the temporal channel, and p controls the mask intensity. The motion-preserving video

$\hat{X}^R \in \mathbb{R}^{T \times H \times W \times 3}$ is subsequently reconstructed from the masked latent representation \hat{Z} . We then derive the binary mask sequence $\zeta \in \mathbb{R}^{T \times H \times W \times 1}$ from \hat{X}^R and apply it to X^R to generate the augmented sample.

Semantic Positive Mining (SPM). While single-modal contrastive learning enables CCL-SLR to extract modality-specific representation, the ‘‘semantic collision’’ problem identified by CrosSCLR [54] remains a significant challenge. The semantic collision occurs during contrastive learning when sample embeddings with high semantic similarity in the memory bank are mistakenly treated as negative examples. In response to this semantic misalignment, we introduce SPM, a mechanism that identifies semantic positive samples across memory banks of different modalities. As shown in Fig. 2 (b), we select the top- k nearest neighbors of g_q^m from \mathcal{M}_f^m as positive samples, while treating the remaining embeddings as negative samples. This selection process generates a binary pseudo-label $y^m \in \mathbb{R}^N$:

$$y^R = \text{Top-}k(g_q^R \cdot \mathcal{M}_g^R), \quad y^P = \text{Top-}k(g_q^P \cdot \mathcal{M}_g^P). \quad (5)$$

To align the neighborhood structure across modalities, we combine y^R and y^P through maximization to obtain the cross-modal binary pseudo-label y . Actually, since the labels are binary, the max function here is equivalent to taking the union of the positive samples from two modalities. The embeddings in \mathcal{M}_f^m serve as classifiers, generating class logits $\hat{y}^m \in \mathbb{R}^N$ that classify f_q^m into N pseudo categories:

$$\hat{y}^m = \phi(f_q^m \cdot \mathcal{M}_f^m / \tau_{spm}), \quad (6)$$

where τ_{spm} denotes the temperature coefficient and $\phi(\cdot)$ is the sigmoid function [51]. Then, \hat{y}^m and y are utilized for binary cross-entropy (BCE) loss:

$$\mathcal{L}_{spm}^m = -\frac{1}{N} \sum_{i=1}^N [y_i \log \hat{y}_i^m + (1 - y_i) \log(1 - \hat{y}_i^m)], \quad (7)$$

Additionally, to perform intra-modal instance discrimination, we formulate the single-modal contrastive loss for both modalities as follows:

$$\mathcal{L}_{cl}^m = \mathcal{L}_{cl}(f_q^m, f_k^m, \mathcal{M}_f^m). \quad (8)$$

The final single-modal contrastive loss is as follows:

$$\mathcal{L}_{single} = \underbrace{\mathcal{L}_{cl}^R + \mathcal{L}_{spm}^R}_{\mathcal{L}^R} + \underbrace{\mathcal{L}_{cl}^P + \mathcal{L}_{spm}^P}_{\mathcal{L}^P}. \quad (9)$$

3.3. Cross-Modal Contrastive Learning

While previous work [49] successfully employed Kullback-Leibler (KL) divergence to maintain distribution consistency within pose modality, cross-modal alignment between pose and RGB modality remains challenging due to their

substantial data distribution gap. To this end, we extend single-modal contrastive learning to the cross-modal domain by directly aligning embeddings from both modalities in the latent space. Specifically, for RGB features f_q^R , we utilize f_k^P as positive samples and embeddings in \mathcal{M}_f^P as negative samples from the pose modality to perform contrastive learning; analogously, the symmetric procedure is applied to pose features. The bidirectional cross-modal contrastive losses are defined as:

$$\mathcal{L}^{R \rightarrow P} = \mathcal{L}_{cl}(f_q^P, f_k^R, \mathcal{M}_f^R), \quad (10)$$

$$\mathcal{L}^{P \rightarrow R} = \mathcal{L}_{cl}(f_q^R, f_k^P, \mathcal{M}_f^P), \quad (11)$$

$$\mathcal{L}_{cross} = \mathcal{L}^{R \rightarrow P} + \mathcal{L}^{P \rightarrow R}. \quad (12)$$

The overall pre-training objective function is formulated as:

$$\mathcal{L} = \mathcal{L}_{single} + \mathcal{L}_{cross}. \quad (13)$$

This pre-training strategy enables CCL-SLR to align embedding spaces across modalities, performing instance discrimination for consistency representation learning.

3.4. Model Details

During pre-training phase, each projection head is a 2-layer MLP which projects the encoder output into a 128-dimensional embedding. During fine-tuning phase, we utilize the query encoders as feature extractors and replace the projection head with a fully connected layer for prediction. In this phase, both branches are optimized via cross-entropy loss. The final prediction is obtained by summing the predicted logits from the RGB and pose branches.

4. Experiments

4.1. Datasets and Evaluation Metrics

We evaluate our method on four public sign language datasets: MSASL [24], WLASL [26], NMFs-CSL [15], and SLR500 [18], utilizing the entire training sets of all four datasets to pre-train our framework.

MSASL is an American sign language (ASL) dataset, comprising 25,513 samples with a vocabulary size of 1,000. It consists of 16,054, 5,287, and 4,172 samples in the training, development (dev), and test set, respectively. Furthermore, it provides subset consisting of only the top 200 most frequent glosses. WLASL is another widely-used ASL dataset with a vocabulary size of 2000. It includes 14,289, 3,916, and 2,878 samples in the training, dev, and test set, respectively. Similar to MSASL, WLASL also releases subset consisting of 300 frequent glosses.

NMFs-CSL is a challenging Chinese sign language (CSL) dataset that incorporates a wide range of fine-grained non-manual features (NMFs). With a vocabulary size of 1,067, the dataset has 25,608 and 6,402 samples in the

Method	Modality		WLASL2000				WLASL300				MSASL1000				MSASL200			
	Pose	RGB	Per-instance		Per-class		Per-instance		Per-class		Per-instance		Per-class		Per-instance		Per-class	
			Top-1	Top-5	Top-1	Top-5	Top-1	Top-5	Top-1	Top-5	Top-1	Top-5	Top-1	Top-5	Top-1	Top-5	Top-1	Top-5
ST-GCN [40]	✓		34.40	66.57	32.53	65.45	44.46	73.05	45.29	73.16	36.03	59.92	32.32	57.15	52.91	76.67	54.20	77.62
I3D [1]		✓	32.48	57.31	-	-	56.14	79.94	-	-	-	-	57.69	81.08	-	-	81.97	93.79
TCK [28]		✓	-	-	-	-	68.56	89.52	68.75	89.41	-	-	-	-	80.31	91.82	81.14	92.24
StepNet [36]		✓	56.89	88.64	54.54	87.97	74.70	91.02	75.32	91.17	-	-	-	-	-	-	-	-
StepNet [‡] [36]		✓	61.17	91.94	58.43	91.43	-	-	-	-	-	-	-	-	-	-	-	-
HMA [14]	✓	✓	51.39	86.34	48.75	85.74	-	-	-	-	69.39	87.42	66.54	86.56	85.21	94.41	86.09	94.42
BEST [46]	✓	✓	54.59	88.08	52.12	87.28	75.60	92.81	76.12	93.07	71.21	88.85	68.24	87.98	86.83	95.66	87.45	95.72
SignBERT [13]	✓	✓	54.69	87.49	52.08	86.93	74.40	91.32	75.27	91.72	71.24	89.12	67.96	88.40	86.98	96.39	87.62	96.43
SignBERT+ [16]	✓	✓	55.59	89.37	53.33	88.82	78.44	94.31	79.12	94.43	73.71	90.12	70.77	89.30	88.08	96.47	88.62	96.47
SAM*(5 [†]) [20]	✓	✓	58.73	91.46	55.93	90.94	-	-	-	-	-	-	-	-	-	-	-	-
SAM-v2*(5 [†]) [21]	✓	✓	59.39	91.48	56.63	90.89	-	-	-	-	-	-	-	-	-	-	-	-
NLA-SLR [55]	✓	✓	61.05	91.45	58.05	90.70	86.23	97.60	86.67	97.81	72.56	89.12	69.86	88.48	88.74	96.17	89.23	96.38
NLA-SLR(3 [†]) [55]	✓	✓	61.26	91.77	58.31	90.91	86.98	97.60	87.33	97.81	73.80	89.65	70.95	89.07	89.48	96.69	89.86	96.93
CCL-SLR (Ours)	✓	✓	62.20	92.39	58.80	91.85	86.28	97.63	86.81	97.87	77.71	92.28	76.27	92.30	90.21	96.47	90.86	96.65

Table 1. Comparison with previous works on WLASL and MSASL datasets. The results of ST-GCN and I3D are reproduced by [13] and [26], respectively. * denotes methods using extra modalities such as optical flow, depth map and depth flow. † denotes a multi-crop inference. ‡ denotes fusion results with optical flow.

Method	Modality		NMFs-CSL		SLR500
	Pose	RGB	Top-1	Top-5	Top-1
ST-GCN* [40]	✓		59.9	86.8	90.0
I3D* [1]		✓	64.4	88.0	-
GLE-Net [15]		✓	69.0	88.1	96.8
StepNet [36]		✓	77.2	92.5	-
StepNet [‡] [36]		✓	83.6	97.0	-
HMA [14]	✓	✓	75.6	95.3	95.9
SignBERT [13]	✓	✓	78.4	97.3	97.6
SignBERT+ [16]	✓	✓	-	-	97.8
BEST [46]	✓	✓	79.2	97.1	97.7
NLA-SLR [55]	✓	✓	83.4	98.3	-
NLA-SLR(3 [†]) [55]	✓	✓	83.7	98.5	-
CCL-SLR (Ours)	✓	✓	84.4	99.3	97.8

Table 2. Comparison with previous works on NMFs-CSL and SLR500 datasets. † denotes a multi-crop inference. ‡ denotes fusion results with optical flow. * represents methods reproduced by [15].

training and test sets. SLR500 is another large-scale CSL dataset that covers 500 common words. It contains a total of 125,000 samples, with 90,000 samples for training and 35,000 samples for testing. Following [13, 55], we report the average accuracy over instances and classes, respectively. Since NMFs-CSL and SLR500 have a balanced distribution with an equal number of samples per class, we only report per-instance accuracy.

4.2. Experimental Settings

The RGB branch applies spatial augmentations including random cropping, horizontal flipping, and color jittering, while the pose branch implements random rotation, scaling, joint masking, and flipping. Both branches share temporal augmentation through random temporal cropping. More de-

tails about data preprocessing, pose encoder and data augmentation are provided in the Appendix.

The temperature hyperparameters τ and τ_{spm} are set to 0.07 and 0.02 respectively. The hyperparameters of MPM α and p are set to 0.5, and 0.2, respectively. During pre-training phase, CCL-SLR is trained for 140 epochs with a learning rate of 0.01 and batch size 64, where the learning rate is divided by 10 at epoch 100. During fine-tuning phase, the model is trained for 40 epochs with learning rate 0.05 and batch size 128, with the learning rate divided by 10 at epochs 25 and 35. An SGD optimizer with 0.9 momentum is utilized throughout the training process. All experiments are conducted on $8 \times$ NVIDIA RTX 3090 GPUs.

4.3. Comparison with State-of-the-art Methods

MSASL. Table 1 presents an extensive comparison of our method against other approaches on two MSASL sub-splits. Benefiting from the consistency modeling between dual modalities during pre-training, our method surpasses the previously best-performing NLA-SLR [55], which utilized semantic information within sign glosses, by 5.15%/1.53% on the 1,000/200 sub-splits, respectively, in terms of per-instance top-1 accuracy.

WLASL. In Table 1, we also illustrates the results on the WLASL dataset. our CCL-SLR achieves a 2.81% improvement in the accuracy of the top-1 per instance compared to SAM-v2 [21], a multi-modal ensemble approach using RGB, pose, optical flow, and depth, demonstrating that alignment of the cross-modal distribution during pre-training enhances the generalization capability.

NMFs-CSL. The comparison on the NMFs-CSL dataset is shown in Table 2. Unlike previous pre-training methods such as SignBERT[13] and BEST[46], which simply fuse RGB predictions in downstream tasks and lack consideration of modeling cross-modal consistency during

\mathcal{L}_{spm}^m	\mathcal{L}_{cross}	MPM	Per-instance		Per-class	
			Top-1	Top-5	Top-1	Top-5
			70.04	88.43	67.73	86.91
✓			71.20	88.93	68.96	88.14
✓	✓		76.27	91.78	74.26	91.57
✓	✓	✓	77.71	92.28	76.27	92.30

Table 3. Ablation studies for the major components of CCL-SLR.

Setting	Per-instance		Per-class	
	Top-1	Top-5	Top-1	Top-5
w/o \mathcal{L}_{cross}	72.69	90.23	79.81	89.46
w/ \mathcal{L}_{cross}	77.71	92.28	76.27	92.30

Table 4. Ablation studies on cross-modal contrastive learning loss.

pre-training. Our method achieves superior performance with 6.0% improvements over SignBERT on NMFs-CSL dataset.

SLR500. Lastly, Table 2 also presents the performance comparison on the SLR500 dataset. On this sufficiently large dataset, self-supervised learning methods such as SignBERT+[16] and BEST[46] achieve more outstanding performance. Similarly, our cross-modal pre-training approach effectively integrates consistency cues from two modalities, achieving a 97.8% Top-1 accuracy.

4.4. Ablation Study

In this section, we conduct several ablation studies to verify the effectiveness of several key components in our proposed framework on the MSASL [48] dataset.

Key Components of CCL-SLR. As shown in Table 3, we conduct ablation studies on three key components of CCL-SLR: Semantic Positive Mining (\mathcal{L}_{spm}^m), cross-modal contrastive learning (\mathcal{L}_{cross}), and Motion-Preserving Masking (MPM). Initially, with a baseline comprising two independent single-modal learning branches, the incorporation of SPM improves top-1 accuracy by 0.85%, which is attributed to semantic positive pairs enforcing cross-modal consistency between sample spaces. The implementation of \mathcal{L}_{cross} further boosts the performance significantly from 74.66% to 76.27%, demonstrating its effectiveness in aligning multi-modal representation during pre-training. Ultimately, by suppressing non-semantic features in RGB videos, the integration of MPM achieves the optimal performance with 77.71% top-1 accuracy.

Cross-Modal Contrastive Learning Loss. As shown in Table 4, we first study the effects of the cross-modal contrastive learning loss \mathcal{L}_{cross} . After removing \mathcal{L}_{cross} from CCL-SLR, the top-1 accuracy significantly drops by about 5%. The reason is that \mathcal{L}_{cross} plays a significantly important role in our framework by explicitly and effec-

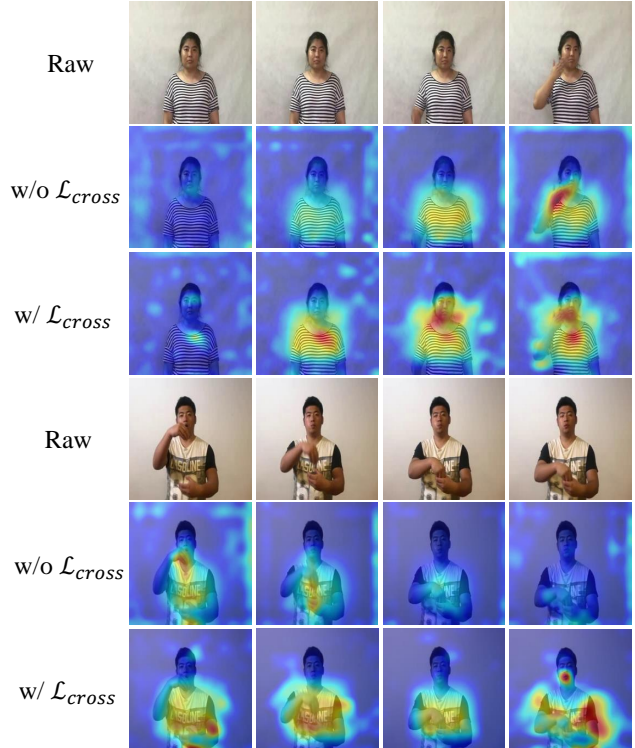


Figure 4. Visualizations of heatmaps by Grad-CAM [35]. Top: raw frames; Middle: heatmaps of the fine-tuning results of the RGB encoder from pre-training without \mathcal{L}_{cross} ; Bottom: heatmaps of the fine-tuning results of the RGB encoder from pre-training with \mathcal{L}_{cross} . The samples are from the NMFs-CSL [15] dataset.

tively aligning the feature spaces between the two modalities, which implicitly helps the model extract cross-modal consistency cues. Additionally, Fig. 4 demonstrates the heatmaps generated by fine-tuning RGB encoder from pre-training with and without \mathcal{L}_{cross} . Especially, performing cross-modal contrastive learning during pretraining allows the RGB branch to learn semantic information from the pose modality. This significantly enhances the model’s attention to non-manual features (yellow and red areas) such as facial expressions and body movements.

Pre-Training Data Scale. In Fig. 5, we explore the impact of the pre-training data scale on the performance of our proposed framework. The experimental results reveal that the performance exhibits a steady improvement as the proportion of the pre-training data scale increases, demonstrating that our model can effectively leverage large-scale unlabeled multi-modal sign language data to enhance its representation capability, thereby indicating the scalability of our approach to large-scale sign language data.

Motion-Preserving Masking. The influence of MPM is explored by sequentially changing the mask probability pa-

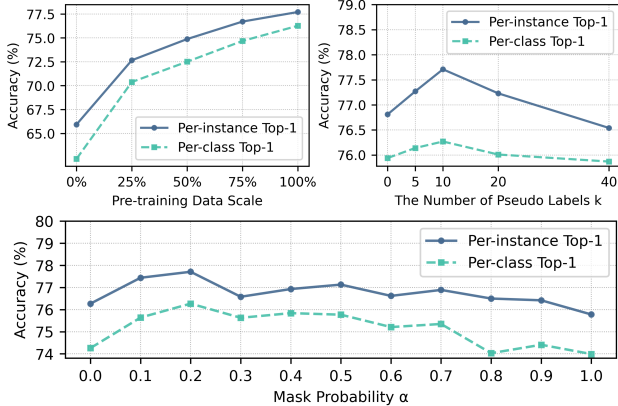


Figure 5. Hyperparameter selection on CCL-SLR performance. We sequentially investigate the impact of the pre-training data scale, the number of pseudo-positive labels k , and the mask probability α .

Setting	Per-instance		Per-class	
	Top-1	Top-5	Top-1	Top-5
\mathcal{M}_f only	76.94	92.01	75.86	92.02
\mathcal{M}_g and \mathcal{M}_f	77.71	92.28	76.27	92.30

Table 5. Ablation studies on cross-modal contrastive learning loss.

Setting	Fine-tuning		Per-instance		Per-class	
	Pose	RGB	Top-1	Top-5	Top-1	Top-5
Baseline	✓		62.96	83.13	60.48	82.60
	✓	✓	60.25	82.78	57.16	80.35
	✓	✓	70.04	88.43	67.73	86.91
CCL-SLR	✓		71.98	89.93	70.04	89.41
	✓	✓	68.14	86.58	65.43	86.21
	✓	✓	77.71	92.28	76.27	92.30

Table 6. Ablation studies for different pre-training modalities.

parameter α within $[0.0, 1.0]$. As shown in Fig. 5, the performance reaches its optimum at $\alpha = 0.2$, suggesting that moderate masking effectively mitigate static bias while preserving essential dynamic information. However, an excessively high mask ratio can lead to performance degradation. Visualization results of MPM are provided in the Appendix. **Semantic Positive Mining.** We investigate the sensitivity of hyperparameter k to our method, which denotes the number of mined semantic positives per modality. As illustrated in Fig. 5, experimental results demonstrate that either extremely small or large values of k lead to performance degradation. Excessively large k value will introduce noise during contrastive learning, which affects the representation capability of the model. According to these empirical results, we determine $k = 10$ as default.

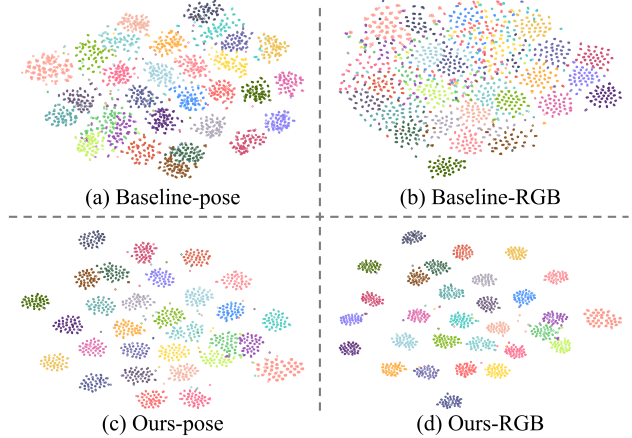


Figure 6. t-SNE visualizations of feature embeddings. We sample 30 sign words from SLR500 dataset and visualize the features extracted from the proposed CCL-SLR and its baseline, respectively.

Why keeping two memory banks? Different from vanilla MoCo v2 [3] framework, we maintain two memory banks (\mathcal{M}_g and \mathcal{M}_f) in our pipeline: one for pseudo-labeling and the other for contrastive learning. Intuitively, maintaining a unique memory bank is structurally more concise. However, according to previous work [9], features before projection are more generally applicable, while features after projection are specialized for the instance discrimination task of contrastive learning. As shown in the Table 5, experimental results also indicate that directly using \mathcal{M}_f for pseudo-labeling leads to a slight performance degradation.

Cross-Modal Consistency Pre-training. As illustrated in Table 6, our framework is pre-trained under two different settings: baseline and CCL-SLR. The baseline conducts pre-training on two single-modal branches without key components of CCL-SLR. Compared with baseline, our CCL-SLR significantly improves the ISLR performance on the MSASL dataset for both single-modal and fusion results, which validates that our method effectively learns consistency representation across modalities. To further validate the effectiveness of our cross-modal consistency learning, t-SNE visualizations of the feature embeddings learned from pre-training are shown in Fig. 6. For both modalities, the representations learned by our CCL-SLR demonstrate more compact clustering patterns compared to the baseline method, indicating the superior representation learning capability of CCL-SLR.

5. Conclusion

In this paper, we investigate the challenge of sign language recognition through multi-modal consistency learning. We propose CCL-SLR, a novel self-supervised pre-training framework that enhances sign representation by leveraging complementary information across modalities. Our framework incorporates two key innovations: MPM,

which enables motion-aware feature extraction from RGB videos, and SPM, which effectively addresses the semantic collision problem in contrastive learning. We conduct comprehensive evaluations on four widely-used ISLR datasets, where CCL-SLR consistently achieves state-of-the-art performance, validating the effectiveness of our proposed approach.

References

- [1] Joao Carreira and Andrew Zisserman. Quo vadis, action recognition? a new model and the kinetics dataset. In *CVPR*, pages 6299–6308, 2017. 2, 6
- [2] Ting Chen, Simon Kornblith, Kevin Swersky, Mohammad Norouzi, and Geoffrey E Hinton. Big self-supervised models are strong semi-supervised learners. *NeurIPS*, pages 22243–22255, 2020. 3
- [3] Xinlei Chen, Haoqi Fan, Ross Girshick, and Kaiming He. Improved baselines with momentum contrastive learning. *arxiv*, 2020. 3, 4, 8
- [4] MMPose Contributors. OpenMMLab Pose Estimation Toolbox and Benchmark. <https://github.com/open-mmlab/mmpose>, 2020. 4
- [5] Shuangrui Ding, Maomao Li, Tianyu Yang, Rui Qian, Hao-hang Xu, Qingyi Chen, Jue Wang, and Hongkai Xiong. Motion-aware contrastive video representation learning via foreground-background merging. In *CVPR*, pages 9716–9726, 2022. 3
- [6] Ali Farhadi, David Forsyth, and Ryan White. Transfer learning in sign language. In *CVPR*, pages 1–8, 2007. 2
- [7] Holger Fillbrandt, Suat Akyol, and K-F Kraiss. Extraction of 3d hand shape and posture from image sequences for sign language recognition. In *2003 IEEE International SOI Conference. Proceedings (Cat. No. 03CH37443)*, pages 181–186, 2003. 2
- [8] Jean-Bastien Grill, Florian Strub, Florent Altché, Corentin Tallec, Pierre Richemond, Elena Buchatskaya, Carl Doersch, Bernardo Avila Pires, Zhaohan Guo, Mohammad Gheshlaghi Azar, et al. Bootstrap your own latent—a new approach to self-supervised learning. *NeurIPS*, pages 21271–21284, 2020. 3
- [9] Kartik Gupta, Thalaisyasingam Ajanthan, Anton van den Hengel, and Stephen Gould. Understanding and improving the role of projection head in self-supervised learning. *arxiv*, 2022. 8
- [10] Kensho Hara, Hirokatsu Kataoka, and Yutaka Satoh. Learning spatio-temporal features with 3d residual networks for action recognition. In *ICCV*, pages 3154–3160, 2017. 2, 4
- [11] Kaiming He, Haoqi Fan, Yuxin Wu, Saining Xie, and Ross Girshick. Momentum contrast for unsupervised visual representation learning. In *CVPR*, pages 9729–9738, 2020. 3
- [12] Geoffrey Hinton. Distilling the knowledge in a neural network. *arxiv*, 2015. 4
- [13] Hezhen Hu, Weichao Zhao, Wengang Zhou, Yuechen Wang, and Houqiang Li. Signbert: Pre-training of hand-model-aware representation for sign language recognition. In *ICCV*, pages 11087–11096, 2021. 1, 2, 3, 6
- [14] Hezhen Hu, Wengang Zhou, and Houqiang Li. Hand-model-aware sign language recognition. In *AAAI*, pages 1558–1566, 2021. 1, 2, 6
- [15] Hezhen Hu, Wengang Zhou, Junfu Pu, and Houqiang Li. Global-local enhancement network for nmf-aware sign language recognition. *ACM TOMM*, 17(3):1–19, 2021. 1, 2, 5, 6, 7
- [16] Hezhen Hu, Weichao Zhao, Wengang Zhou, and Houqiang Li. Signbert+: Hand-model-aware self-supervised pre-training for sign language understanding. *IEEE TPAMI*, 45(9):11221–11239, 2023. 1, 2, 3, 6, 7
- [17] Jie Huang, Wengang Zhou, Houqiang Li, and Weiping Li. Sign language recognition using 3d convolutional neural networks. In *ICME*, pages 1–6. IEEE, 2015. 1
- [18] Jie Huang, Wengang Zhou, Houqiang Li, and Weiping Li. Attention-based 3D-CNNs for large-vocabulary sign language recognition. *IEEE TCSVT*, 29(9):2822–2832, 2018. 1, 5
- [19] Sangryul Jeon, Dongbo Min, Seungryong Kim, and Kwanghoon Sohn. Mining better samples for contrastive learning of temporal correspondence. In *CVPR*, pages 1034–1044, 2021. 3
- [20] Songyao Jiang, Bin Sun, Lichen Wang, Yue Bai, Kunpeng Li, and Yun Fu. Skeleton aware multi-modal sign language recognition. In *CVPR*, pages 3413–3423, 2021. 2, 6
- [21] Songyao Jiang, Bin Sun, Lichen Wang, Yue Bai, Kunpeng Li, and Yun Fu. Sign language recognition via skeleton-aware multi-model ensemble. *arxiv*, 2021. 1, 2, 3, 6
- [22] Tao Jiang, Peng Lu, Li Zhang, Ning Ma, Rui Han, Chengqi Lyu, Yining Li, and Kai Chen. RTMPose: Real-time multi-person pose estimation based on mmpose. *arxiv*, 2023. 12
- [23] Sheng Jin, Lumin Xu, Jin Xu, Can Wang, Wentao Liu, Chen Qian, Wanli Ouyang, and Ping Luo. Whole-body human pose estimation in the wild. In *ECCV*, 2020. 12
- [24] Hamid Reza Vaezi Joze and Oscar Koller. Ms-asl: A large-scale data set and benchmark for understanding american sign language. *arxiv*, 2018. 1, 2, 5
- [25] Oscar Koller, Sepehr Zargaran, Hermann Ney, and Richard Bowden. Deep sign: Enabling robust statistical continuous sign language recognition via hybrid cnn-hmms. *IJCV*, 126:1311–1325, 2018.
- [26] Dongxu Li, Cristian Rodriguez, Xin Yu, and Hongdong Li. Word-level deep sign language recognition from video: A new large-scale dataset and methods comparison. In *CVPR*, pages 1459–1469, 2020. 1, 5, 6
- [27] Dongxu Li, Xin Yu, Chenchen Xu, Lars Petersson, and Hongdong Li. Transferring cross-domain knowledge for video sign language recognition. In *CVPR*, pages 6205–6214, 2020. 2
- [28] Dongxu Li, Xin Yu, Chenchen Xu, Lars Petersson, and Hongdong Li. Transferring cross-domain knowledge for video sign language recognition. In *CVPR*, pages 6205–6214, 2020. 1, 6
- [29] Dongxu Li, Chenchen Xu, Liu Liu, Yiran Zhong, Rong Wang, Lars Petersson, and Hongdong Li. Transcribing natural languages for the deaf via neural editing programs. In *AAAI*, pages 11991–11999, 2022. 1, 2
- [30] Ji Lin, Chuang Gan, and Song Han. Tsm: Temporal shift module for efficient video understanding. In *ICCV*, pages 7083–7093, 2019. 2
- [31] Hadi Mohaghegh Dolatabadi, Sarah Erfani, and Christopher Leckie. Advflow: Inconspicuous black-box adversarial attacks using normalizing flows. *NeurIPS*, pages 15871–15884, 2020. 4
- [32] Sylvie CW Ong and Surendra Ranganath. Automatic sign language analysis: A survey and the future beyond lexical

- meaning. *IEEE Trans. Pattern Anal. Mach. Intell.*, 27(06): 873–891, 2005. [2](#)
- [33] Alec Radford, Jong Wook Kim, Chris Hallacy, Aditya Ramesh, Gabriel Goh, Sandhini Agarwal, Girish Sastry, Amanda Askell, Pamela Mishkin, Jack Clark, et al. Learning transferable visual models from natural language supervision. In *ICML*, pages 8748–8763, 2021. [3](#)
- [34] Razieh Rastgoo, Kouros Kiani, and Sergio Escalera. Sign language recognition: A deep survey. *Expert Systems with Applications*, 164:113794, 2021. [2](#)
- [35] Ramprasaath R. Selvaraju, Michael Cogswell, Abhishek Das, Ramakrishna Vedantam, Devi Parikh, and Dhruv Batra. Grad-cam: Visual explanations from deep networks via gradient-based localization. In *ICCV*, pages 618–626, 2017. [7](#)
- [36] Xiaolong Shen, Zhedong Zheng, and Yi Yang. Stepnet: Spatial-temporal part-aware network for isolated sign language recognition. *ACM TOMM*, 20(7):1–19, 2024. [2, 6](#)
- [37] Thad Starner. *Visual recognition of american sign language using hidden markov models*. PhD thesis, Massachusetts Institute of Technology, 1995. [2](#)
- [38] Jue Wang, Gedas Bertasius, Du Tran, and Lorenzo Torresani. Long-short temporal contrastive learning of video transformers. In *CVPR*, pages 14010–14020, 2022. [3](#)
- [39] Ning Xu, Linjie Yang, Yuchen Fan, Dingcheng Yue, Yuchen Liang, Jianchao Yang, and Thomas Huang. Youtube-vos: A large-scale video object segmentation benchmark. *arxiv*, 2018. [4](#)
- [40] Sijie Yan, Yuanjun Xiong, and Dahua Lin. Spatial temporal graph convolutional networks for skeleton-based action recognition. In *AAAI*, 2018. [6](#)
- [41] Sijie Yan, Yuanjun Xiong, and Dahua Lin. Spatial temporal graph convolutional networks for skeleton-based action recognition. In *AAAI*, pages 1–10, 2018. [12](#)
- [42] Haoyuan Zhang, Yonghong Hou, Wenjing Zhang, and Wanqing Li. Contrastive positive mining for unsupervised 3d action representation learning. In *ECCV*, pages 36–51, 2022. [3](#)
- [43] Hao Zhang, Feng Li, Shilong Liu, Lei Zhang, Hang Su, Jun Zhu, Lionel M Ni, and Heung-Yeung Shum. Dino: Detr with improved denoising anchor boxes for end-to-end object detection. *arXiv*, 2022. [3](#)
- [44] Jihai Zhang, Wengang Zhou, Chao Xie, Junfu Pu, and Houqiang Li. Chinese sign language recognition with adaptive hmm. In *ICME*, pages 1–6. IEEE, 2016. [1](#)
- [45] Manlin Zhang, Jinpeng Wang, and Andy J Ma. Suppressing static visual cues via normalizing flows for self-supervised video representation learning. In *AAAI*, pages 3300–3308, 2022. [3](#)
- [46] Weichao Zhao, Hezhen Hu, Wengang Zhou, Jiabin Shi, and Houqiang Li. Best: Bert pre-training for sign language recognition with coupling tokenization. In *AAAI*, pages 3597–3605, 2023. [1, 2, 3, 6, 7](#)
- [47] Weichao Zhao, Hezhen Hu, Wengang Zhou, Yunyao Mao, Min Wang, and Houqiang Li. Masa: Motion-aware masked autoencoder with semantic alignment for sign language recognition. *IEEE TCSVT*, 34(11):10793–10804, 2024. [2](#)
- [48] Weichao Zhao, Wengang Zhou, Hezhen Hu, Min Wang, and Houqiang Li. Self-supervised representation learning with spatial-temporal consistency for sign language recognition. *arxiv*, 2024. [1, 2, 3, 7](#)
- [49] Weichao Zhao, Wengang Zhou, Hezhen Hu, Min Wang, and Houqiang Li. Self-supervised representation learning with spatial-temporal consistency for sign language recognition. *IEEE TIP*, 33:4188–4201, 2024. [5](#)
- [50] Wengang Zhou, Weichao Zhao, Hezhen Hu, Zecheng Li, and Houqiang Li. Scaling up multimodal pre-training for sign language understanding. *arXiv preprint arXiv:2408.08544*, 2024. [4, 12](#)
- [51] Feng Zhu, Hongsheng Li, Wanli Ouyang, Nenghai Yu, and Xiaogang Wang. Learning spatial regularization with image-level supervisions for multi-label image classification. In *CVPR*, pages 5513–5522, 2017. [5](#)
- [52] Ke Zhu, Minghao Fu, and Jianxin Wu. Multi-label self-supervised learning with scene images. In *ICCV*, pages 6694–6703, 2023. [3](#)
- [53] Yisheng Zhu, Hu Han, Zhengtao Yu, and Guangcan Liu. Modeling the relative visual tempo for self-supervised skeleton-based action recognition. In *ICCV*, pages 13913–13922, 2023. [3](#)
- [54] Mohammadreza Zolfaghari, Yi Zhu, Peter Gehler, and Thomas Brox. Crossclr: Cross-modal contrastive learning for multi-modal video representations. In *ICCV*, pages 1450–1459, 2021. [3, 5](#)
- [55] Ronglai Zuo, Fangyun Wei, and Brian Mak. Natural language-assisted sign language recognition. In *CVPR*, pages 14890–14900, 2023. [1, 2, 6](#)

Cross-Modal Consistency Learning for Sign Language Recognition

Supplementary Material

A. Framework Implementation

In this section, we describe the details of the pose data extraction, the encoder architecture in the pose branch and data preprocessing.

A.1. Pose Keypoint Extraction.

We employ RTMPose-x [22] from MMPose to extract 133 whole-body keypoints, which provide detailed spatial information for subsequent pose analysis. The visualization of whole-body keypoints are shown in Figure 7. We select 75 keypoints and divide the keypoints into several sub-pose (left hand, right hand, face, mouth, and body). We select the indices for the left hand ($\{92-112\}$), right hand ($\{113-133\}$), face ($\{24-41, 54\}$), mouth ($\{84-92\}$) and body ($\{0,5,7,9,6,8,10\}$) to represent each group (denoted as $\mathcal{G}_r, r \in \{LH, RH, F, M, B\}$).

A.2. Encoder of Pose Branch.

We utilize a GCN+Transformer architecture [50] as the pose branch encoder. Specifically, four ST-GCN modules [41] are employed to extract group-specific features \mathbf{v}_r from pose group \mathcal{G}_r , where the left and right hands share the same module for feature extraction. The extracted 512 dimension features are then concatenated into manual features \mathbf{v}_{man} and non-manual features \mathbf{v}_{non} :

$$\mathbf{v}_{man} = \text{Concat}([\mathbf{v}_{LH}, \mathbf{v}_{RH}, \mathbf{v}_B]), \quad (14)$$

$$\mathbf{v}_{non} = \text{Concat}([\mathbf{v}_F, \mathbf{v}_M]), \quad (15)$$

where $\mathbf{v}_{LH}, \mathbf{v}_{RH}, \mathbf{v}_B, \mathbf{v}_F$, and \mathbf{v}_M represent features from left hand, right hand, body, face, and mouth, respectively. To model temporal relationships, two separate 3-block 8-head Transformers (\mathcal{T}_{man} and \mathcal{T}_{non}) are leveraged to process these features and generate the final pose embedding:

$$\mathbf{v} = \text{Concat}([\mathcal{T}_{man}(\mathbf{v}_{man}), \mathcal{T}_{non}(\mathbf{v}_{non})]), \quad (16)$$

where final pose embedding \mathbf{v} is 1024 dimensions.

A.3. Data Preprocessing.

For data preprocessing, we select aforementioned 75 keypoints for pose input per frame and resize all RGB frames to 224×224 . For computational efficiency, we uniformly sample $T = 32$ frames from each sequence.

A.4. Data Augmentation

For the query and key samples, we ensure consistency in hyperparameters during data augmentation while performing the process independently. For random temporal cropping,

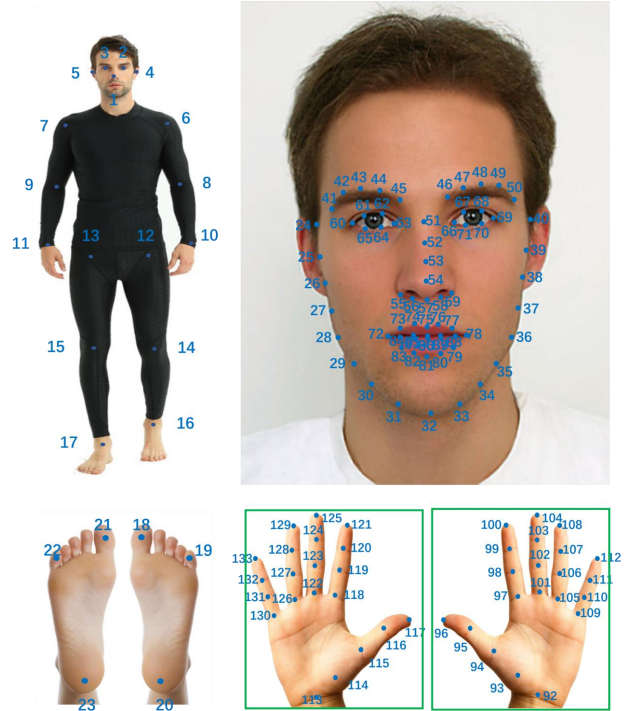
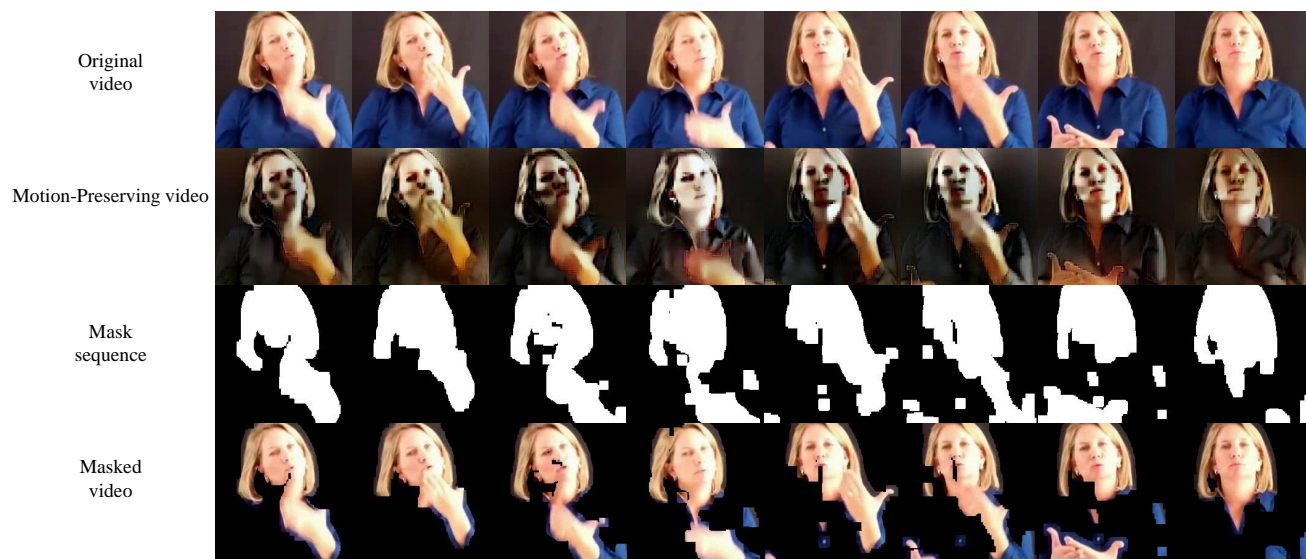


Figure 7. The visualization of the whole-body 133 keypoints from [23].

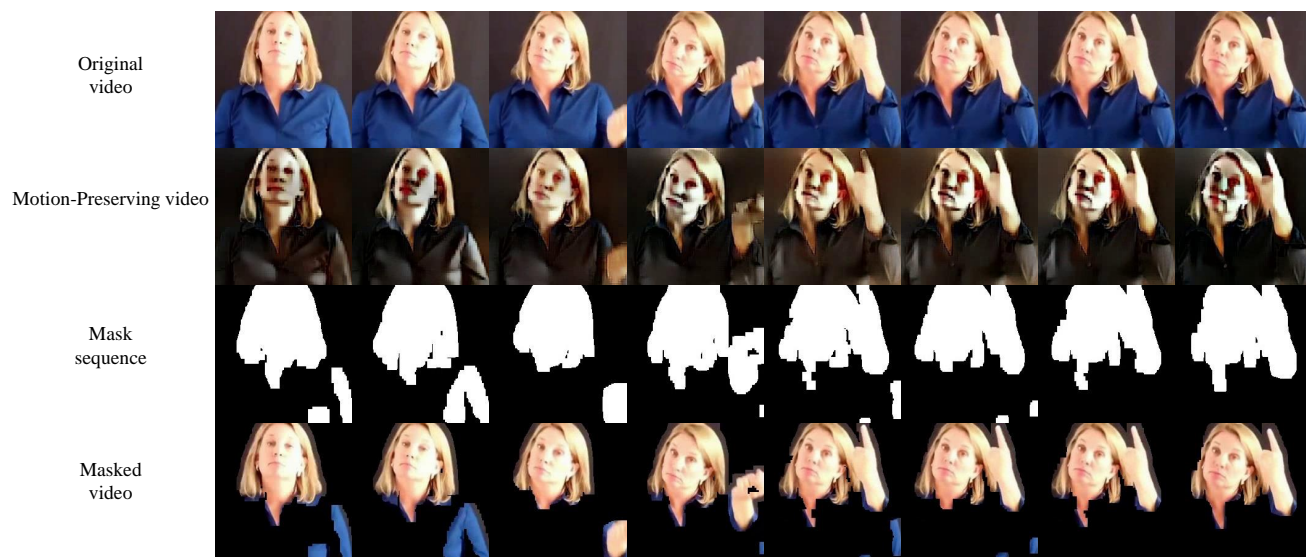
we first apply continuous temporal cropping to the input sequence, randomly extracting a clip from the interval $[lT, T]$ frames. Subsequently, we uniformly sample a fixed number of K frames from the cropped interval. In our approach, we set $l = 0.1$ and $K = 64$.

B. Visualization of Motion-Preserving Masking

As shown in Fig. 8 and Fig. 9, the generated motion-preserving videos effectively suppress static regions while highlighting motion areas. Furthermore, since motion-preserving videos significantly alter the pixel distribution of the original videos, we further generate binary motion-preserving mask sequences from the motion-preserving videos. These mask sequence are applied to mask original videos, explicitly mitigating static information redundancy in RGB modality. The visualizations indicate that MPM preserves semantically informative regions such as hand and facial features, while effectively suppressing semantically irrelevant areas including clothing textures and background elements, enhancing the cross-modal feature alignment between pose and RGB representations.



(a) Label: good

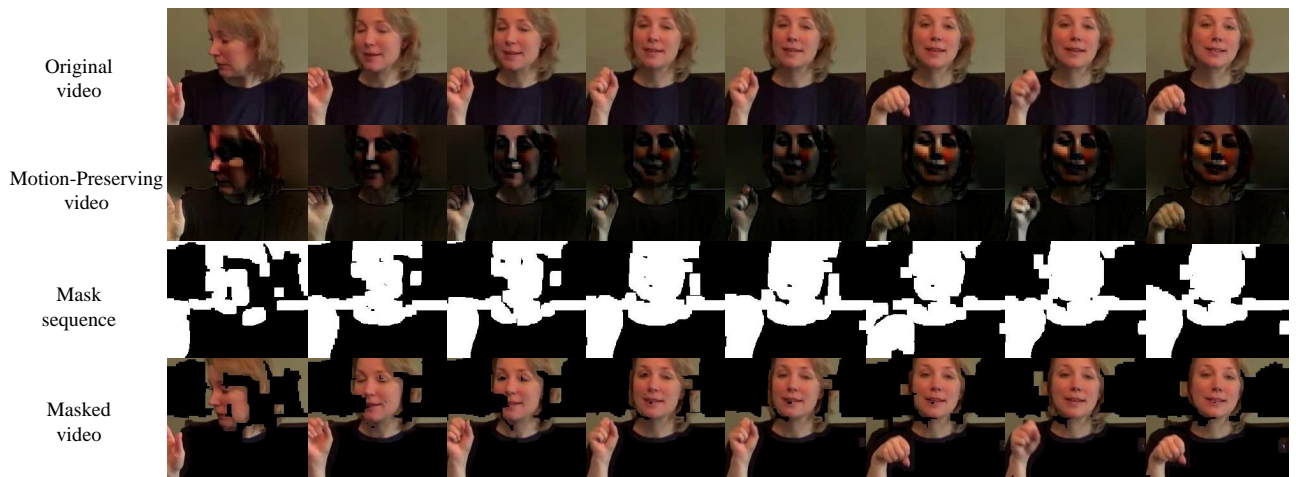


(b) Label: understand

Figure 8. The visualizations of motion-preserving masking.



(a) Label: wow



(b) Label: yes

Figure 9. The visualizations of motion-preserving masking.